CHEMISTRY OF MATERIALS
Article

Chem. Mater. **2009,** *21,* 5335–5342 5335
DOI:10.1021/cm902639p

Noncentrosymmetric Polar Oxide Material, Pb_3SeO_5: Synthesis, Characterization, Electronic Structure Calculations, and Structure−Property Relationships

Sang-Hwan Kim, Jeongho Yeon, and P. Shiv Halasyamani*

Department of Chemistry, University of Houston, 136 Fleming Building, Houston, Texas 77204-5003

Received August 26, 2009. Revised Manuscript Received September 29, 2009

A noncentrosymmetric (NCS) polar compound, Pb_3SeO_5, has been hydrothermally synthesized and structurally characterized by single crystal X-ray diffraction. Pb_3SeO_5 exhibits a two-dimensional crystal structure consisting of layers of α-PbO-like "slabs" that are linked through SeO_3 polyhedra. Structurally, it is the bridging SeO_3 polyhedra between the α-PbO-like slabs that results in the NCS and polar nature of Pb_3SeO_5. Powder second-harmonic generation (SHG) measurements using 1064 nm radiation indicates that Pb_3SeO_5 exhibits a strong SHG efficiency of ∼300 × α-SiO_2. Additional SHG measurements indicate the material is type-I phase-matchable. Converse piezoelectric measurements revealed a d_{33} value of ∼81 pm/V, and a pyroelectric coefficient of $-42\ \mu C/(m^2\ K)$ at 65 °C was also determined. Using first principle density functional theory (DFT) calculations, we demonstrated that polarization reversal in Pb_3SeO_5 is not energetically favorable—the material is polar but *not* ferroelectric. Our calculations also indicate that both Pb^{2+} and Se^{4+} cations exhibit a stereoactive lone-pair. In addition, differential scanning calorimetry measurements revealed an irreversible phase transition at ∼440 °C. Finally, infrared, UV−vis and thermogravimetric measurements were also performed. Crystal data: Pb_3SeO_5, orthorhombic, space group $Cmc2_1$ (no. 36), a = 10.5211(13) Å, b = 10.7151(13) Å, c = 5.7452(7) Å, V = 647.68(14) Å^3, and Z = 2.

Introduction

Understanding the origin of asymmetry in noncentrosymmetric (NCS) solid-state materials[1] is critically important as it would enable us to design new materials exhibiting technologically relevant physical properties such as ferroelectricity and pyroelectricity.[2−5] These properties are directly related to macroscopic polarization changes and are intimately correlated to the NCS crystal classes.[6,7] In order to exhibit ferroelectricity or pyroelectricity, all materials must crystallize in one of ten polar crystal classes, 1, 2, 3, 4, 6, *m*, *mm*2, 3*m*, 4*mm*, or 6*mm*.[8] Common asymmetric building units in NCS oxide materials include distorted MO_6 octahedra (M = d^0 transition metal cation: Ti^{4+}, Nb^{5+}, W^{6+}, etc.)[9−14] as well as asymmetric AO_xE polyhedra (A = lone-pair cation: Se^{4+}, I^{5+}, Pb^{2+}, etc. and E = lone-pair).[15−28] *Microscopically*, these polyhedra exhibit dipole moments that when aligned result in a *macroscopically* polar NCS material. With respect to the MO_6 and AO_xE polyhedra, second-order Jahn−Teller (SOJT) effects have been invoked to explain the local polar coordination environments of the d^0 transition metal

(1) Preiser, C.; Losel, J.; Brown, I. D.; Kunz, M.; Skowron, A. *Acta Crystallogr., Sect. B* **1999**, *B55*, 698.
(2) Auciello, O.; Scott, J. F.; Ramesh, R. *Phys. Today* **1998**, *51*, 22.
(3) Haertling, G. H. *J. Am. Ceram. Soc.* **1999**, *82*, 797.
(4) Lang, S. B.; Das-Gupta, D. K. Pyroelectricity: Fundamentals and Applications. In *Handbook of Advanced Electronic and Photonic Materials and Devices*; Nalwa, H. S., Ed.; Academic Press: San Francisco, 2001; Vol. *4*, pp 1−55.
(5) Lang, S. B. *Phys. Today* **2005**, *58*, 31.
(6) Nye, J. F. *Physical Properties of Crystals*; Oxford University Press: Oxford, 1957.
(7) Halasyamani, P. S.; Poeppelmeier, K. R. *Chem. Mater.* **1998**, *10*, 2753.
(8) Hahn, T. *International Tables for Crystallography, Volume A, Space Group Symmetry*; Kluwer Academic: Dordrecht, Holland, 2006; Vol. A.
(9) Abrahams, S. C.; Hamilton, W. C.; Reddy, J. M. *J. Phys. Chem. Solids* **1966**, *27*, 1013.
(10) Jamieson, P. B.; Abrahams, S. C. *Acta Crystallogr., Sect. B* **1968**, *24*, 984.
(11) Jamieson, P. B.; Abrahams, S. C.; Bernstein, J. L. *J. Chem. Phys.* **1969**, *50*, 4352.
(12) Goodenough, J. B. *Annu. Rev. Mater. Sci.* **1998**, *28*, 1.
(13) Halasyamani, P. S. *Chem. Mater.* **2004**, *16*, 3586.
(14) Sun, C.-F.; Hu, C.-L.; Xu, X.; Ling, J.-B.; Hu, T.; Kong, F.; Long, X.-F.; Mao, J.-G. *J. Am. Chem. Soc.* **2009**, *131*, 9486.
(15) Bergman, J. G.; Crane, G. R. *J. Solid State Chem.* **1975**, *12*, 172.
(16) Galy, J.; Meunier, G.; Andersson, S.; Astrom, A. *J. Solid State Chem.* **1975**, *13*, 142.
(17) Raveau, B. *Rev. Silicon, Germanium, Tin Lead Compd.* **1982**, *6*, 287.
(18) Serezhkin, V. N.; Buslaev, Y. A. *Zh. Neorg. Khim.* **1997**, *42*, 1180.
(19) Serezhkin, V. N.; Serezhkin, L. B.; Furmanova, N. G.; Buslaev, Y. A. *Zh. Neorg. Khim.* **1997**, *42*, 1879.
(20) Porter, Y.; Ok, K. M.; Bhuvanesh, N. S. P.; Halasyamani, P. S. *Chem. Mater.* **2001**, *13*, 1910.
(21) Ok, K. M.; Bhuvanesh, N. S. P.; Halasyamani, P. S. *Inorg. Chem.* **2001**, *40*, 1978.
(22) Ok, K. M.; Halasyamani, P. S. *Inorg. Chem.* **2005**, *44*, 2263.
(23) Kong, F.; Huang, S.-P.; Sun, Z.-M.; Mao, J.-G.; Cheng, W.-D. *J. Am. Chem. Soc.* **2006**, *128*, 7750.
(24) Barrier, N.; Malo, S.; Hernandez, O.; Hervieu, M.; Raveau, B. *J. Solid State Chem.* **2006**, *179*, 3484.
(25) Mayerova, Z.; Johnsson, M.; Lidin, S. *Angew. Chem., Int. Ed.* **2006**, *45*, 5602.
(26) Rieger, F.; Mudring, A.-V. *Inorg. Chem.* **2007**, *46*, 446.
(27) Mao, J.-G.; Jiang, H.-L.; Kong, F. *Inorg. Chem.* **2008**, *47*, 8498.
(28) Chang, H.-Y.; Kim, S.-H.; Ok, K. M.; Halasyamani, P. S. *J. Am. Chem. Soc.* **2009**, *131*, 6865.

Published on Web 10/12/2009

and lone-pair cation.[12,29−34] Deeper insight with respect to lone-pair formation in heavier p-metal cations such as Tl^{+}, Pb^{2+}, and Bi^{3+} has been reported experimentally.[35] Theoretical examinations of their electronic structures through comparing hypothetical symmetric and experimental NCS crystal structures revealed that the stereoactive lone-pair formation is primarily driven by the interactions between the s- and p-orbitals in the metal cation and oxide anions, respectively, and not solely by intra-atomic sp-orbital mixing of the cations.[36−39] The interactions are thought to be mediated through cation or anion p-orbitals in low-lying unoccupied states. Despite the great success regarding the elucidation of the local asymmetry, the reasons why the asymmetric polyhedra sometimes align in solid-state structures is often unclear.

With extended solid-state materials such as ANa-$NbOF_5$ ($A = K^{+}$ or Cs^{+}), Poeppelmeier et al. have reported that different cation−anion interactions in the bond network result in NCS polar and centrosymmetric nonpolar structures.[40] We recently reported that the A^{+} cation in $A_2Ti(IO_3)_6$ ($A = Li^{+}$, Na^{+}, K^{+}, Rb^{+}, Cs^{+}, or Tl^{+}) is a dominant factor in the material's macroscopic polarity.[41] Materials in the $PbO-SeO_2$ system are of interest attributable to the occurrence of lone-pairs on Pb^{2+} and Se^{4+}. Ternary oxides in this system include $PbSeO_3$, $PbSe_2O_5$, Pb_3SeO_5, and Pb_5SeO_7,[42−45] and of these, only Pb_3SeO_5 is NCS and polar. No functional properties with respect to the polarity of Pb_3SeO_5 have been reported. In this paper, we not only report on the synthesis and structure of Pb_3SeO_5, but we also investigate the material's functional properties—second-harmonic generation, piezoelectricity, ferroelectricity, and pyroelectricity. In addition, electronic structure calculations have been performed to examine the local polarity associated with Pb^{2+} and Se^{4+}, i.e., their lone-pair, as well as the macroscopic polarity observed in Pb_3SeO_5. Our calculations indicate that the local polarity in Pb_3SeO_5 is energetically very unfavorable toward reversibility—the material is pyroelectric and *not* ferroelectric. From the direct space analyses, stereoactive lone-pairs are observed near all the cations. We also examined the thermal properties and observed an irreversible phase transition at around 440 °C. This transition is unexpected since it has been reported that Pb_3SeO_5 is stable from 470 to 610 °C and is formed through the thermal dissociation of $PbSeO_3$.[42] In this paper, we report on the synthesis, structure, functional properties, and electronic structure characterization, as well as infrared, thermogravimetric, and differential scanning calorimetry measurements of Pb_3SeO_5.

Table 1. Crystallographic Data for Pb_3SeO_5

formula	Pb_3SeO_5
fw (g/mol)	780.53
T (K)	296.0(2)
λ (Å)	0.71073
crystal system	orthorhombic
space group	$Cmc2_1$ (no. 36)
a (Å)	10.5211(13)
b (Å)	10.7151(13)
c (Å)	5.7452(7)
V (Å^3)	647.68(14)
Z	4
ρ_{calcd} (g/cm^3)	8.007
μ (mm^{-1})	83.357
$2\theta_{max}$ (deg)	57.4
R(int)	0.0687
GOF(F^2)	1.031
$R(F)^a$	0.0301
$R_w(F_o^2)^b$	0.0509
Flack param	0.04(2)

^{a} $R(F) = \Sigma||F_o| - |F_c||/\Sigma|F_o|$. ^{b} $R_w(F_o^2) = [\Sigma w(F_o^2 - F_c^2)^2/\Sigma w(F_o^2)^2]^{1/2}$.

Experimental Section

Reagents. PbO (Aldrich, 99.9%), SeO_2 (Alfa Aesar, 99%), and NaOH (Aldrich, 99%) were used as received.

Synthesis. Pb_3SeO_5 was hydrothermally synthesized by combining 1.00 g (4.50 mmol) of PbO and 0.50 g (4.50 mmol) of SeO_2 with 8 mL of 1 M NaOH(aq). The mixture was placed in a 23-mL Teflon-lined autoclave that was subsequently sealed. The autoclave was gradually heated to 230 °C, held for 2 days, and cooled slowly to room temperature at a rate 6 °C/h. The mother liquor was decanted, and the product, transparent colorless rod-shaped crystals, was recovered by filtration and washed with excess amounts of distilled water and acetone. The colorless rod-shaped crystals were obtained in nearly quantitative yield.

Single Crystal X-ray Diffraction. A colorless rod-shaped crystal ($0.02 \times 0.02 \times 0.08$ mm^3) was chosen for single-crystal X-ray collection. The data were collected using a Siemens SMART APEX diffractometer equipped with a 1 K CCD area detector using graphite-monochromated Mo Kα radiation. A hemisphere of data was collected using a narrow-frame method with scan widths of 0.30° in ω, and an exposure time of 60s per frame. The data were integrated using the Siemens SAINT program,[46] with the intensities corrected for Lorentz-Polarization, air absorption, and absorption attributable to the variation in the path length through the detector face plate. Psi-scans were used for the absorption correction on the data.

(29) Opik, U.; Pryce, M. H. L. *Proc. R. Soc. London, Ser. A* **1957**, *238*, 425.
(30) Bader, R. F. W. *Mol. Phys.* **1960**, *3*, 137.
(31) Bader, R. F. W. *Can. J. Chem.* **1962**, *40*, 1164.
(32) Pearson, R. G. *J. Mol. Struct.: THEOCHEM* **1983**, *103*, 25.
(33) Pearson, R. G. *J. Am. Chem. Soc.* **1969**, *91*, 4947.
(34) Wheeler, R. A.; Whangbo, M. H.; Hughbanks, T.; Hoffmann, R.; Burdett, J. K.; Albright, T. A. *J. Am. Chem. Soc.* **1986**, *108*, 2222.
(35) Payne, D. J.; Egdell, R. G.; Walsh, A.; Watson, G. W.; Guo, J.; Glans, P. A.; Learmonth, T.; Smith, K. E. *Phys. Rev. Lett.* **2006**, *96*, 157403/1.
(36) Watson, G. W.; Parker, S. C. *J. Phys. Chem. B* **1999**, *103*, 1258.
(37) Seshadri, R.; Hill, N. A. *Chem. Mater.* **2001**, *13*, 2892.
(38) Mudring, A.-V.; Rieger, F. *Inorg. Chem.* **2005**, *44*, 6240.
(39) Stoltzfus, M. W.; Woodward, P.; Seshadri, R.; Park, J.-H.; Bursten, B. *Inorg. Chem.* **2007**, *46*, 3839.
(40) Marvel, M. R.; Lesage, J.; Baek, J.; Halasyamani, P. S.; Stern, C. L.; Poeppelmeier, K. R. *J. Am. Chem. Soc.* **2007**, *2007*, 13963.
(41) Chang, H. Y.; Kim, S.-H.; Ok, K. M.; Halasyamani, P. S. *Chem. Mater.* **2009**, *21*, 1654.
(42) Lahtinen, M.; Valkonen, J. *Chem. Mater.* **2002**, *14*, 1812.
(43) Zlomanov, V. P.; Popovkin, B. A.; Tananaeva, O. I.; Novoselova, A. V. *Zh. Neorg. Khim.* **1962**, *7*, 2746.
(44) Popovkin, B. A.; Novoselova, A. V. *Dokl. Akad. Nauk SSSR* **1961**, *139*, 117.
(45) Krivovichev, S. V.; Avdontseva, E. Y.; Burns, P. C. *Z. Anorg. Allg. Chem.* **2004**, *630*, 558.
(46) SAINT Program for Area Detector Absorption Correction, 4.05; Siemens Analytical X-ray Systems, Inc.: Madison, WI, 1995.
(47) Sheldrick, G. M. *SHELXTL DOS/Windows/NT, 5.10*; Bruker Analytical X-Ray Instruments, Inc.: Madison, WI., 1997.
(48) Sheldrick, G. M. *SHELXS-97 - A program for automatic solution of crystal structures*; University of Goettingen: Goettingen, Germany, 1997.

Table 2. Atomic Coordinates and Equivalent Isotropic Displacement Parameters (Å) for Pb_3SeO_5

	x	y	z	U_{eq}[a]
Pb(1)	0.0000	0.38218(4)	0.9461(3)	0.01257(19)
Pb(2)	−0.24759(3)	0.61215(3)	0.95133(10)	0.01469(15)
Se	0.0000	0.12986(12)	0.3990(3)	0.0106(4)
O(1)	−0.1345(4)	0.4957(10)	0.715(2)	0.0133(12)
O(2)	0.0000	0.2788(7)	0.491(2)	0.022(2)
O(3)	0.1284(6)	0.0708(6)	0.5417(10)	0.0193(15)

[a] U_{eq} is defined as one-third of the trace of the orthogonalized U_{ij} tensor.

Table 3. Selected Bond Distances (Å) in Pb_3SeO_5

Pb(1)−O(1) × 2	2.291(9)	Pb(2)−O(1)	2.195(10)
Pb(1)−O(1) × 2	2.470(10)	Pb(2)−O(1)	2.246(10)
		Pb(2)−O(3)	2.411(6)
		Pb(2)−O(3)	2.727(6)
Se−O(2)	1.681(9)		
Se−O(3) × 2	1.703(6)		

The data were solved by direct and refined against F^2 by full-matrix least-squares techniques using SHELXS-97 and SHELXL-97, respectively.[47−49] All of the atoms in the structure were refined with anisotropic thermal parameters, and the refinements converged for $I > 2\sigma(I)$. The Flack parameter was refined to 0.04(2). The structure was checked for missing symmetry elements using PLATON.[50] Relevant crystallographic data, atomic coordinates and thermal parameters, and selected bond distances for Pb_3SeO_5 are given in Tables 1, 2, and 3, respectively.

Powder X-ray Diffraction. Powder X-ray diffraction (PXRD) data were collected using a PANalytical X'Pert PRO diffractometer using Cu Kα radiation. The 2θ range was 5−90° with a step size of 0.0167° and a fixed time of 0.2s. The PXRD pattern is in good agreement with the calculated PXRD from the single crystal model (see Figure S1 of the Supporting Information). From the thermogravimetric and differential scanning calorimetric studies (see below), we observed a phase transition at ∼440 °C.

Thermogravimetric Analysis. Thermogravimetric analysis was carried out on a TGA 951 thermogravimetric analyzer (TA Instruments). The sample was placed in a platinum crucible and heated at a rate of 10 °C min^{-1} from room temperature to 900 °C under flowing nitrogen. The TGA data has been deposited in the Supporting Information (see Figure S2).

Differential Scanning Calorimetry Analysis. Differential scanning calorimetry (DSC) analysis was performed on an EXSTAR6000 Differential Scanning Calorimeter (SII NanoTechnology Inc.). A 10.0 mg portion of the sample was placed in an aluminum pan covered by an aluminum lid that was heated (cooled) at a rate of 10 °C min^{-1} between 25 and 500 °C under flowing air. Alumina was used as the reference during the measurements.

Infrared Spectroscopy. Infrared spectra were recorded on a Matteson FTIR 5000 spectrometer in the 400−3000 cm^{-1} range (see Figure S3 in the Supporting Information). The IR spectra revealed Pb−O (Se−O) vibrations at 457 cm^{-1} (435, 515, 726, and 790 cm^{-1}) consistent with published reports.[51−53]

UV−vis Diffuse Reflectance Spectroscopy. UV−visible reflectance data were collected on a Varian Cary 500 scan UV−vis-NIR spectrophotometer over the 200−1500 nm spectral range at room temperature. Poly(tetrafluoroethylene) was used as a reference material. The reflectance spectrum was converted to absorbance using the Kubelka−Munk function (see Figure S4 in the Supporting Information).[54,55]

Second Harmonic Generation (SHG). Powder SHG measurements were performed on a modified Kurtz-NLO[56] system using a pulsed Nd:YAG laser with a wavelength of 1064 nm. A detailed description of the equipment and methodology has been published.[57] The SHG efficiency has been shown to depend strongly upon particle size,[56] thus polycrystalline samples were ground and sieved into distinct particle size ranges (20−45, 45−63, 63−75, 75−90, >90 μm). In order to make relevant comparisons with known SHG materials, crystalline α-SiO_2 and $LiNbO_3$ were also ground and sieved into the same particle size ranges. No index matching fluid was used in any of the experiments.

Piezoelectric Measurements. Converse piezoelectric measurements were performed using a Radiant Technologies RT66A piezoelectric test system with a TREK (model 609×10^{-6}) high-voltage amplifier, Precision Materials Analyzer, Precision High-Voltage Interface, and MTI 2000 Fotonic Sensor. Pb_3SeO_5 was pressed into 12-mm diameter, ∼1-mm-thick pellets using a cold isostatic press at 3500 psi at room temperature, after which the material was heated to 300 °C for 7 days. Initially silver paste was applied on both sides of the pellet. Upon curing at 200 °C, we observed a black residue that penetrated the pellet. As such, gold was deposited on both sides of a fresh pellet with silver applied on top of the gold. This pellet was cured at 200 °C for 3 h. Solely using gold was not possible attributable to the poor optical sensitivity in measuring the converse piezoelectricity. A maximum voltage of 30 kV/cm was applied to the sample.

Polarization Measurements. The pellet used in the piezoelectric measurements was used in the polarization measurements. The polarization was measured on a Radiant Technologies RT66A Ferroelectric Test System with a TREK high voltage amplifier between room temperature and 165 °C in Delta 9023 environmental test chamber. The unclamped pyroelectric coefficient, defined as dP/dT (change in the polarization with respect to the change in temperature), was determined by measuring the polarization as a function of temperature. A detailed description of the methodology used has been published elsewhere.[57] To determine the ferroelectric behavior, the polarization loop was measured at room temperature under a static electric field of 13−30 kV/cm in the 5−200 Hz frequency range. For the pyroelectric measurements, the polarization was measured statically from room temperature to 165 °C in 20 °C increments, with an electric field of 30 kV/cm. The temperature was allowed to stabilize before the polarization was measured.

Electronic Structure Calculations. First principle electronic band structure calculations were performed with the plane wave pseudopotential[58] and tight-binding linear muffin-tin orbital (TB-LMTO)[59,60] methods based upon density functional theory (DFT).[61,62]

(49) Sheldrick, G. M. *SHELXL-97 - A program for crystal structure refinement*; University of Goettingen: Goettingen, 1997.
(50) Spek, A. L. *PLATON*; Utrecht University: Utrecht, The Netherlands, 2001.
(51) Adams, D. M.; Stevens, D. C. *J. Chem. Soc., Dalton Trans.* **1977**, 1096.
(52) Gospodinov, G. G.; Sukova, L. M.; Petrov, K. I. *Zh. Neorg. Khim.* **1988**, *33*, 1970.
(53) Sammes, N. M.; Tompsett, G.; Cartner, A. M. *J. Mater. Sci.* **1995**, *30*, 4299.
(54) Kubelka, P.; Munk, F. Z. *Tech. Phys.* **1931**, *12*, 593.
(55) Tauc, J. *Mater. Res. Bull.* **1970**, *5*, 721.
(56) Kurtz, S. K.; Perry, T. T. *J. Appl. Phys.* **1968**, *39*, 3798.
(57) Ok, K. M.; Chi, E. O.; Halasyamani, P. S. *Chem. Soc. Rev.* **2006**, *35*, 710.
(58) Pickett, W. E. *Comput. Phys. Rep.* **1989**, *9*, 115.
(59) Tank, R. W. J. O.; Burckhardt. A.; Andersen, O. K. *TB-LMTO-ASA program*, Version 4.7c; Max-Planck Institute für Festkörperforschung: Stuttgart, Germany, 1994.
(60) Andersen, O. K. *Phys. Rev. B* **1975**, *12*, 3060.
(61) Hohenberg, P.; Kohn, W. *Phys. Rev.* **1964**, *136*, B864.
(62) Kohn, W.; Sham, L. J. *Phys. Rev.* **1965**, *140*, A1133.

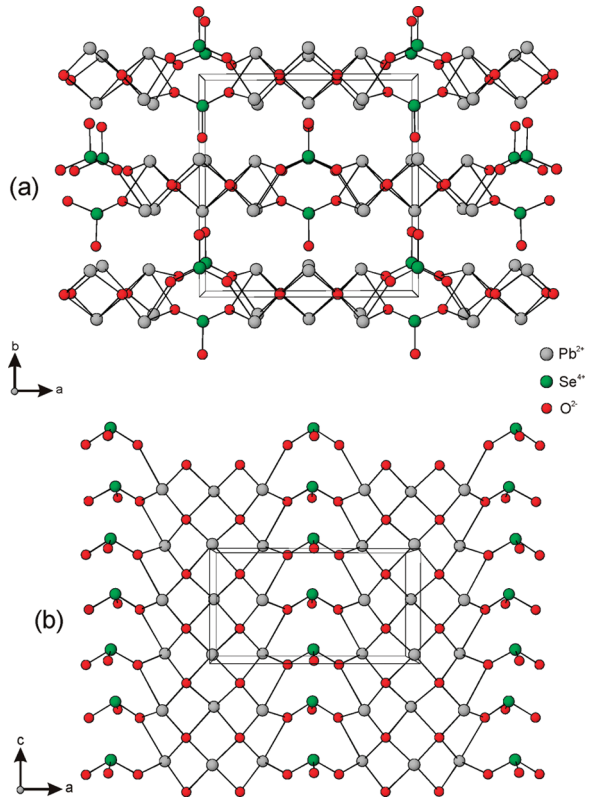

Figure 1. Ball-and-stick representations of the Pb_3SeO_5 crystal structure in the *ab*-plane (a) and *ac*-plane (b). Note in part b that the polar SeO_3 polyhedra are aligned.

As implemented in the Quantum ESPRESSO (4.0.3 version) package,[63] we initially utilized ultrasoft pseudopotentials (USPPs)[64] for all the elements to perform structural optimization with the generalized gradient approximation (GGA)[65] for the exchange-correlation corrections. All ions were relaxed until the Hellmann−Feynman force,[66] and the total energy changes were less than 10^{-3} Rydberg (Ry) per atomic unit (a.u.) and 10^{-4} Ry, respectively, between two consecutive self-consistent field steps. During the relaxations, the experimental symmetry of the structure was retained. A plane wave energy cutoff was set to 37 Ry. A Gaussian smearing of 0.01 Ry for Brillouin zone integrations was adopted with a 4×4×6 *k*-point mesh in the C-centered orthorhombic unit cell. The relaxed structure was adopted in the TB-LMTO calculations within the atomic sphere approximation (ASA). The von Barth-Hedin local exchange-correlation potential was used for the local density approximation (LDA).[67] The radial scalar relativistic Dirac equation was solved for obtaining the partial waves. A total of 9 empty spheres were necessary to achieve space filling for Pb_3SeO_5. A total of 168 irreducible *k*-points from $8 \times 8 \times 8$ grid was used for Brillouin zone integrations by the tetrahedron method.[68,69] The basis set consisted of Pb-6s/6p/[5d]/[5f], Se-4s/4p/[4d] and O-2s/2p orbitals where the orbital in bracket was treated with the downfolding technique.[70] Total energy changes of less than 10^{-5} Ry indicated self-consistency.

Results and Discussion

Crystal Structure Description. As the structure of Pb_3SeO_5 has already been reported, only a brief description will be given here. Pb_3SeO_5 exhibits a two-dimensional layered crystal structure, consisting of linked PbO_4 and SeO_3 polyhedra (see Figure 1a). The layers consist of "trimer slabs" of α-PbO-like PbO_4 polyhedra that are connected by SeO_3 groups (see Figure 1b). As we will discuss later, understanding the structural relationships between the reported material and α-PbO are critical to understanding the macroscopic polarity in Pb_3SeO_5. The trimer slabs consist of edge-shared PbO_4 polyhedra that are linked along the *a*- and *c*-axes. The bridging SeO_3 polyhedra are aligned in a parallel manner along the *c*-axis. Both unique Pb^{2+} cations are bonded to four oxygen atoms with Pb−O distances ranging from 2.194(10) to 2.727(5) Å, whereas the Se^{4+} cations is bonded to three oxygen atoms with Se−O distances ranging from 1.681(9) to 1.703(6) Å. In connectivity terms, the structure may be written as $\{[Pb(1)O_{4/4}]^0\ 2[Pb(2)O_{2/4}O_{2/3}]^{-1/3}\ [SeO_{1/1}O_{2/3}]^{+2/3}\}^0$. The local coordination of both Pb^{2+} and Se^{4+} are highly asymmetric attributable to their stereoactive lone-pair (see Figure 2). More details regarding the lone-pair will be given in the Electronic Structure Analysis section.

One of the most interesting features of Pb_3SeO_5 is its structural relationship to α-PbO. α-PbO is a layered material consisting of edge-shared and puckered PbO_4 polyhedra.[71] The Pb^{2+} cations exhibit a stereoactive lone-pair rendering each PbO_4 polyhedron polar. Within each layer the Pb^{2+} polarization alternates direction, between "up" and "down", resulting in a nonpolar centrosymmetric structure. This is exactly what is observed in the α-PbO section of Pb_3SeO_5. In Pb_3SeO_5, the α-PbO slabs are also pseudocentrosymmetric and are found as trimers—effectively "Pb_3O_3" (3 × α-PbO) units. These pseudocentrosymmetric "Pb_3O_3 slabs" are connected by the polar SeO_3 polyhedra (see Figure 3). In Figure 3, the bridging SeO_3 polyhedra are surrounded by a dotted blue box. Thus, Pb_3SeO_5 may be thought of being built-up as, Pb_3O_3 (3 × α-PbO) + $SeO_2 \rightarrow Pb_3SeO_5$. The bridging SeO_3 polyhedra are not only *locally* polar, but are also aligned in a parallel manner rendering Pb_3SeO_5 *macroscopically* polar. The question remains, however, what factors lead to the SeO_3 polyhedra aligning in a parallel manner. To address this question, we used DFT calculations on a variety of hypothetical Pb_3SeO_5 crystal structures, i.e., those where the SeO_3 polyhedra are antiparallel (see the Electronic Structure Analysis section).

Functional Properties. We investigated the SHG, piezoelectric, and polarization properties of Pb_3SeO_5. Powder SHG measurements on sieved Pb_3SeO_5 revealed an

(63) Baroni, S.; DalCorso, A.; de Gironcoli, S.; Giannozzi, P.; Cavazzoni, C.; Ballabio, G.; Scandolo, S.; Chiarotti, G.; Focher, P.; Pasquarello, A.; Laasonen, K.; Trave, A.; Car, R.; Marzari, N.; Kokalj, A. http://www.quantum-espresso.org/ (accessed October 7, 2009).
(64) Vanderbilt, D. *Phys. Rev. B* **1990**, *41*, 7892.
(65) Perdew, J. P.; Burke, K.; Ernzerhof, M. *Phys. Rev. Lett.* **1996**, *77*, 3865.
(66) Bendt, P.; Zunger, A. *Phys. Rev. Lett.* **1983**, *50*, 1684.
(67) Von Barth, U.; Hedin, L. *J. Phys. C: Solid State Phys.* **1972**, *5*, 1629.
(68) Jepsen, O.; Andersen, O. K. *Solid State Commum.* **1971**, *9*, 1763.
(69) Jepsen, O.; Andersen, O. K. *Phy. Rev. B* **1984**, *29*, 5965.
(70) Lambrecht, W. R. L.; Andersen, O. K. *Phys. Rev. B* **1986**, *34*, 2439.
(71) Dickinson, R. G.; Friauf, J. B. *J. Am. Chem. Soc.* **1924**, *46*, 2457.

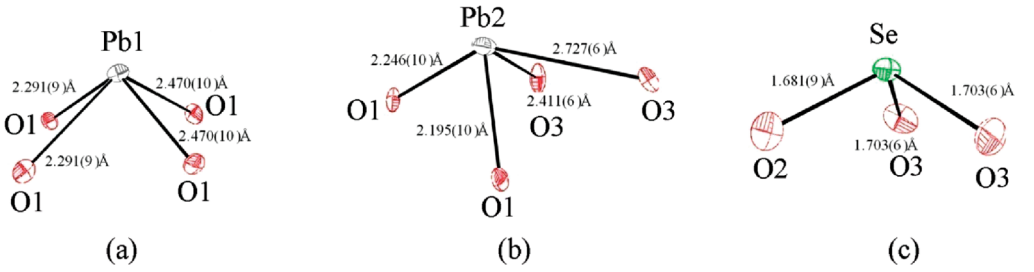

Figure 2. ORTEP diagrams (50% probability ellipsoids) for the (a) $Pb(1)O_4$, (b) $Pb(2)O_4$, and (c) SeO_3 polyhedra. Bond lengths are given next to each metal−oxygen bond.

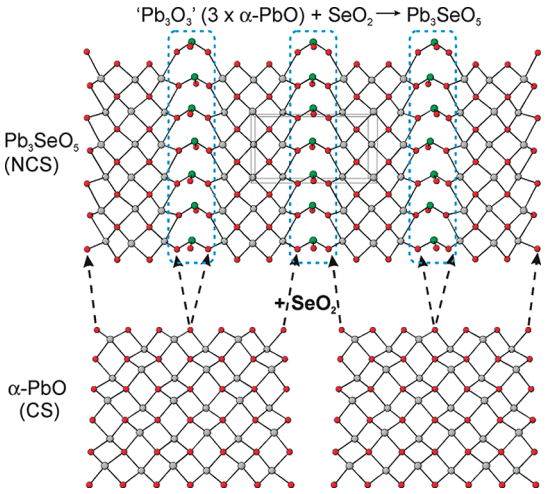

Figure 3. Ball-and-stick representations of a layer of noncentrosymmetric Pb_3SeO_5 (top) and centrosymmetric α-PbO (bottom) are shown. Pb_3SeO_5 may be thought of as pseudocentrosymmetric trimer α-PbO slabs connected by SeO_3 polyhedra (blue box). Note that it is the alignment of the SeO_3 polyhedra that renders Pb_3SeO_5 macroscopically polar.

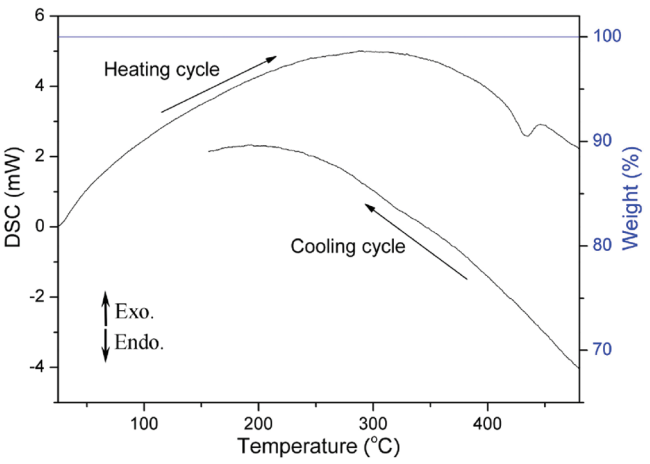

Figure 4. Thermogravimetric (TG) and differential scanning calorimetry (DSC) data for Pb_3SeO_5. The TG data (blue solid line) shows no weight loss up to ~650 °C. In the DSC data (black solid line), an irreversible endothermic peak during the heating cycle at ~440 °C is observed.

efficiency of ~300 × α-SiO_2 in the 45−63 mm particle size range. This efficiency is comparable to $BaTiO_3$ (400 × α-SiO_2) and $LiNbO_3$ (600 × α-SiO_2).[56]

Additional SHG measurements indicate Pb_3SeO_5 is type 1 phase-matchable (see Figure S5 in the Supporting Information), with a $\langle d_{eff} \rangle$ of ~22 pm/V. Converse piezoelectric measurements were also performed and revealed a d_{33} value of ~81 pm/V (see Figure S6 in the Supporting Information). The charge constant compares well to other selenites, such as $LiH_3(SeO_3)_2$ (d_{33} = 46 pC/N).[72] Thus Pb_3SeO_5 represents a rare example of a piezoelectric selenite. As Pb_3SeO_5 is polar, ferroelectric and pyroelectric measurements were performed. Although ferroelectric-like polarization loops were observed (see Figure S7 in the Supporting Information), and their polarization magnitudes were frequency dependent, Pb_3SeO_5 is *not* ferroelectric. The observed loops are attributable to dielectric loss, and not polarization reversal.[73,74] This indicates that the macroscopic polarization in Pb_3SeO_5 cannot be "flipped" in the presence of an external electric field. Macroscopic polarization irreversibility implies microscopic polarization irreversibility, thus it is relevant to examine the local polarization associated with the PbO_4 and SeO_3 polyhedra. As noted earlier and seen in Figure 3, the PbO_4 polyhedral polarizations are pointed in opposite directions. Thus, all of the polarization associated with Pb^{2+} cancels. This is not the situation with the SeO_3 polyhedra. Also, as seen in Figure 3, the SeO_3 polyhedral polarizations are aligned in a parallel manner. If polarization reversal was to occur in Pb_3SeO_5, the polarization associated with the SeO_3 polyhedra would have to be reversed. As we will discuss in the Electronic Structure Analysis section, the SeO_3 polarization reversal is energetically very unfavorable. Pyroelectric measurements revealed a pyroelectric coefficient of −42 μC/(m^2 K) at 65 °C (see Figure S8 in the Supporting Information). The value is consistent with polar materials that are not ferroelectric, such as ZnO (−9.4 μC/(m^2 K)), tourmaline (−4.0 μC/(m^2 K)), and $Li_2Ti(IO_3)_6$ (−2.4 μC/(m^2 K)).[5,75]

Thermal Studies. The thermal stability of Pb_3SeO_5 was investigated through thermogravimetric (TGA) and differential scanning calorimetry (DSC). A phase transition or separation was observed initially when pellets of Pb_3SeO_5 were sintered at 450 °C, as additional peaks were observed in the PXRD pattern (see Figure S1 in the Supporting Information). It should be noted that there

(72) Berlincourt, D.; Cook, W. R. Jr.; Rander, M. E. *Acta Crystallogr.* **1963**, *16*, 163.
(73) Scott, J. F. *J. Phys.: Condens. Matter* **2008**, *20*, 021001/1.
(74) Loidl, A.; Krohns, S.; Hemberger, J.; Lunkenheimer, P. *J. Phys.: Condens. Matter* **2008**, *20*, 191001/1.
(75) Chang, H.-Y.; Kim, S.-H.; Halasyamani, P. S.; Ok, K. M. *J. Am. Chem. Soc.* **2009**, *131*, 2426.

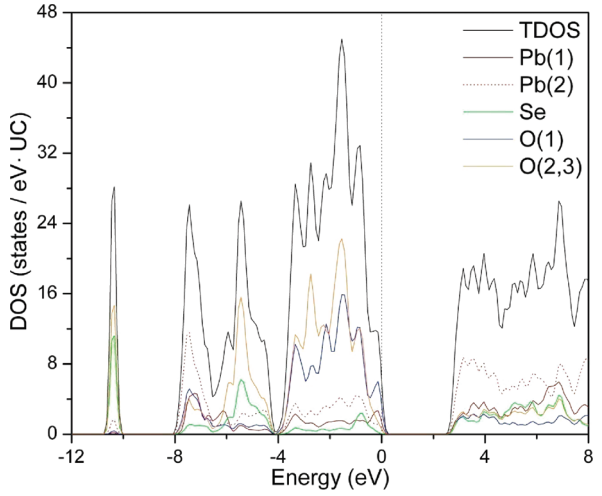

Figure 5. TDOS and PDOSs of Pb_3SeO_5 from the ultrasoft pseudopotential calculations. The vertical dotted line at 0 eV indicates the Fermi level: (black solid line) TDOS; (brown solid line) Pb(1) PDOS; (brown dotted line) Pb(2) PDOS; (green) Se PDOS; (blue) O(1) PDOS; (orange) O(2,3) PDOS.

was no color change in the sample. The TGA data indicated Pb_3SeO_5 is stable to ~600 °C, after which the material rapidly loses SeO_2 and PbO (see Figure S2 in the Supporting Information). DSC measurements revealed an irreversible endothermic peak at ~440 °C in the heating cycle (see Figure 4). As seen in Figure 4, this peak is not observed in the cooling cycle. Powder XRD measurements revealed additional peaks, and SHG measurements indicated the material was no longer SHG active. We are currently investigating the identity of this phase.

Electronic Structure Analysis. The electronic band structure of Pb_3SeO_5 was performed using ultrasoft pseudopotential calculations. For the calculations, we used the relaxed structure self-consistently achieved as mentioned previously. The relaxed and experimental atomic positions and bond distances are in good agreement (see Table S1 in the Supporting Information). Figure 5 shows the total density of states (TDOS) and projected density of states (PDOSs) between −12 and +6 eV. An energy gap of ~2.75 eV is calculated and confirms the insulating nature of the material. The calculated and experimentally determined energy gaps are in good agreement. Overall, a narrow and two broad bands are observed at ~−10 eV and from ~−8 eV to the Fermi level, E_F, respectively. The broad bands are separated by a narrow energy gap around −4 eV. The two broad bands can be separated into upper, ~4 eV to E_F, and lower, ~−8 to −4 eV, bands. In order to resolve the individual atomic contributions, additional detailed PDOSs analyses were performed (see Figure 6) where the top, middle, and bottom panels reveal the Se-(4s,4p), O-(2s,2p), and Pb-(6s,6p) PDOSs. The narrow band at ~−10 eV is mainly composed of Se-4s and O(2,3)-2sp orbitals with a very small contribution from the Pb(2)-6sp orbitals. The broad bands mainly consist of Se-4p, O-2p, Pb-6s, and Pb-6p orbitals. The Se-PDOSs indicate that significant contribution of the Se-4p orbital appears in the top part of the lower band, ~−6.5 to ~−4 eV. In the Pb-PDOS,

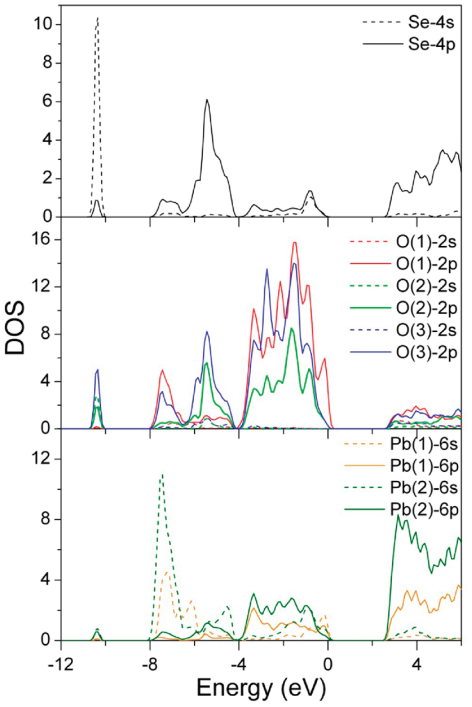

Figure 6. Detailed PDOSs of Se (top), O (middle), and Pb (bottom) from the ultrasoft pseudopotential calculations. The Fermi level is set to 0 eV.

larger and smaller Pb-6s orbital contributions appear in the lower band, ~−8 to ~−4 eV, and near the top part of the upper band, ~−1 eV to E_F, respectively. Conversely, larger and smaller Pb-6p contributions are observed in the upper, −4 eV to E_F, and lower bands. Overall, the Pb(1) and Pb(2) PDOSs are similar to each other but the Pb(2)-6s orbital contribution is slightly shifted toward the lower energy region. In the O-PDOS, the O(1,3)-2p orbitals are dominant in the bottom part of the lower band, ~−8 to ~6.5 eV, whereas the O(2,3)-2p orbitals are dominant at the top part of the lower band, ~−6.5 to ~−4 eV. Each of the O-2p orbitals contributes equally in the upper band, ~−4 to ~−0.5 eV, except for the top part of the upper band, ~−0.5 eV to E_F, which is mainly composed of contributions from the O(1)-2p orbital. These differences in the O- and Pb-PDOSs can be explained by the Se−O and Pb−O bonds (see Table 3), since these bonds influence their relative O-2p and Pb-6s orbital contributions. The contribution of the O(1)-PDOS is very small in the narrow band, ~−10 eV, and in the top part of the lower band, ~−6.5 to −4 eV, since O(1) is not bonded to Se^{4+}. O(1) is bonded to both Pb(1) and Pb(2) and forms the shorter bond with Pb(2). As a result, the O(1)-2p PDOS is dominant in the vicinity of E_F, and the Pb(2)-6s PDOS is slightly shifted to lower energies. O(2) makes very long contacts with both Pb cations, thus the contribution of the O(2)-2p PDOS is negligible in the bottom part of the lower band. O(3) links Se with Pb(2), thus the O(3)-2p orbital contribution is significant in all the bands below E_F.

We also examined the bonding character of the bands through crystal orbital Hamilton population (COHP)

(76) Dronskowski, R.; Bloechl, P. E. *J. Phys. Chem.* **1993**, *97*, 8617.

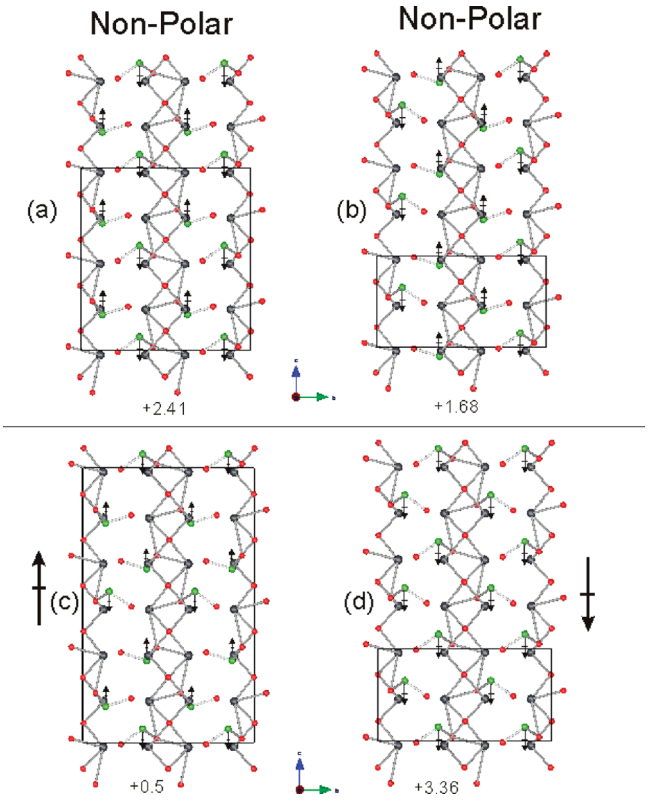

Figure 7. Ball-and-stick representations of four hypothetical Pb_3SeO_5 structures in the *bc*-plane with differently aligned SeO_3 polyhedra. The a and b structures are nonpolar and centrosymmetric, whereas c and d are polar. The macroscopic polarization direction is given in parts c and d. The unit cells are doubled and tripled in parts a and c, respectively. The relative energies, in electronvolts per unit cell, of the hypothetical structures compared to the experimental structure are given at the bottom of each part of the figure.

analyses.[76] The −COHPs for the Se−O and Pb−O (< 3.0 Å) were carried out using TB-LMTO-ASA methods. These calculations also provided qualitatively equivalent TDOS and PDOSs in comparison to those calculated by the pseudopotential method. The −COHP curve for the Se−O shows that the bands above (below) ∼−3 eV to E_F contain nonbonding (bonding) characters of the Se−O(2,3) bonds (see Figure S9 in the Supporting Information) attributable to strong sp-mixing of the Se orbitals. Overall, the −COHP for the Pb−O bonds is similar to Pb−O in α-PbO, where a lone-pair is observed.[77] Similarly, we expect lone-pair formation on the Pb^{2+} and Se^{4+} cations (see the Direct Space Analysis section).

In order to investigate the parallel alignment of the SeO_3 polyhedra, we created four hypothetical Pb_3SeO_5 structures wherein the PbO framework is constant, but the alignment of the SeO_3 polyhedra vary (see Figure 7). Recall that Pb_3SeO_5 is macroscopically polar which is attributable to the parallel alignment of the locally polar SeO_3 polyhedra. In Figure 7, ball-and-stick presentations of four hypothetical Pb_3SeO_5 structures are shown. In all of the hypothetical structures, the local coordination of Pb^{2+} and Se^{4+} is the same as in the experimentally determined Pb_3SeO_5 structure. The total energy for each

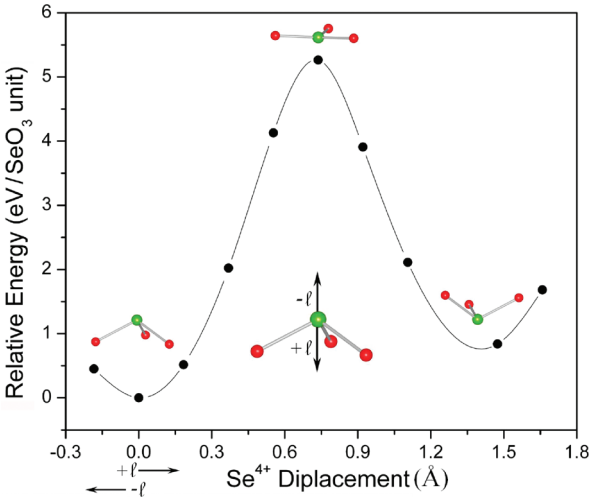

Figure 8. Energy landscape with respect to the Se^{4+} displacement for the inversion of the SeO_3 polyhedra. The calculations (●) were performed, as described in the text, with the Se^{4+} cation moving in the +/ direction. The energy barrier to inversion is ∼5.3 eV.

structure was calculated using the ultrasoft pseudopotential method described earlier. With the hypothetical structures, two are nonpolar (Figure 7a and b) and two are polar (Figure 7c and d). In fact the structure shown in Figure 7d has all the SeO_3 polyhedra inverted relative to the experimentally determined structure. In addition, the unit cells in the structures shown in Figure 7a and c are doubled and tripled respectively to accommodate the SeO_3 inversion scheme. The relative energies of the hypothetical structures compared to the experimental structure are also given in Figure 7. As seen all of the hypothetical structures are energetically less stable than the experimentally determined Pb_3SeO_5. Interestingly, this instability increases proportional to the number of SeO_3 polyhedra that are inverted, i.e., the most unstable structure in Figure 7d has all of the SeO_3 polyhedra inverted. By inverting the SeO_3 polyhedra, the distance between the Se^{4+} and Pb^{2+} cations are decreased, increasing the energetically unfavorable Se^{4+} lone-pair−Pb^{2+} lone-pair interactions. Although additional hypothetical structures can be envisioned, we anticipate that any structures with inverted SeO_3 polyhedra would be energetically unstable attributed to these lone-pair−lone-pair interactions.

It is also important to investigate and understand why Pb_3SeO_5 although polar, is not ferroelectric, i.e., the macroscopic polarization is not reversible. Since the PbO framework in Pb_3SeO_5 is pseudocentrosymmetric—all of the PbO_4 dipole moments point in equal and opposite directions—any possible polarization reversal may be attributed solely to the SeO_3 polyhedra. There are two polarization reversal "mechanisms" that do not involve breaking Se−O bonds. One is similar to the NO_2 group in ferroelectric $NaNO_2$.[78] In this mechanism, the SeO_3 group rotates parallel to the base of the polyhedron. Such a rotation would involve large movements of not

(77) Raulot, J.-M.; Baldinozzi, G.; Seshadri, R.; Cortona, P. *Solid State Sci.* **2002**, *4*, 467.

(78) Sawada, S.; Nomura, S.; Fujii, S. i.; Yoshida, I. *Phys. Rev. Lett.* **1958**, *1*, 320.

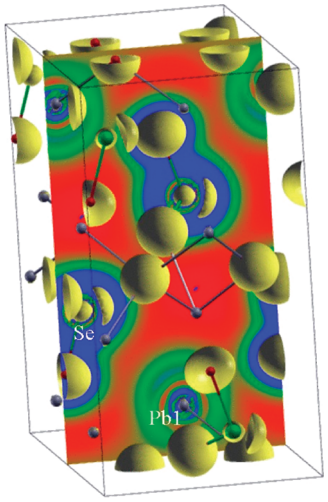

Figure 9. Electron density (ED) isosurface (yellow) at 1 $e^-/Å^3$ and contour map of (100) plane with RGB basis between 0 (red) and 0.375 $e^-/Å^3$ (blue).[78] The stereoactive lone-pairs on the Se^{4+} and Pb^{2+} are clearly observed. The plot was calculated using the TB-LMTO-ASA method.

only the oxide ligands, but also the lone-pair, and is thus considered highly unlikely. The second mechanism is an umbrella-type inversion of the SeO_3 polyhedron—similar to NH_3. We performed frozen phonon calculations in order to evaluate how the total energy would vary during the hypothetical umbrella-type inversion.[28] In these calculations, the Se^{4+} cation was displaced parallel to the pseudo-3-fold axis in the SeO_3 polyhedron. Figure 8 reveals the energy landscape for the SeO_3 polyhedron with respect to the Se^{4+} displacement. The movement of the Se^{4+} toward the base of the SeO_3 polyhedron is $+/$, whereas displacement in the opposite direction is $-/$. Two energy minima and one maximum are observed. The two minima correspond to the relative energies of the experimental and inverted SeO_3 polyhedra. The energy of the inverted SeO_3 polyhedra is raised by ~0.8 eV compared to the original attributable to energetically unfavorable interactions between the Pb^{2+} and Se^{4+} cations. In the inverted structure, these cations are closer to each other. The maximum corresponds to the energy barrier for inversion and is ~5.3 eV—comparable to the IO_3 inversion in $Li_2Ti(IO_3)_6$.[28] This energy barrier is substantially higher than those found in well-known ferroelectrics such as $BaTiO_3$ (~1.8×10^{-2} eV) and $PbTiO_3$ (~2.0×10^{-1} eV).[79] This clearly demonstrates why Pb_3SeO_5 is not ferroelectric, as the polarization reversal of the SeO_3 polyhedra is energetically very unfavorable, i.e., nearly 500 and 45 times the energy required for $BaTiO_3$ and $PbTiO_3$, respectively.

Direct Space Analysis. As described in the previous section, stereoactive lone-pairs are expected to occur on the Se^{4+} and Pb^{2+} cations. To visualize these lone-pairs, electron localization functions (ELFs) and electron density (ED) calculations were performed using the TB-LMTO-ASA method. Figure 9 gives a plot of the ED iso-surface and (100) contour map. The ED iso-surface plotted at 1 $e^-/Å^3$ and between 0 and 0.375 $e^-/Å^3$ clearly reveals highly asymmetric lobes on the Se^{4+} and Pb^{2+} cations, respectively. These asymmetric lobes may be thought of as stereoactive lone-pairs and are consistent with our ELF calculations where lobe-like iso-surfaces, with $\eta = 0.85$, are clearly observed near the cations (see Figure S10 in the Supporting Information). With the lone-pairs, we also consider any relevant lone-pair−lone-pair interactions. The Se^{4+} and $Pb^{2+}(1)$ lone-pairs are perpendicular to each other and are at a distance of ~2.7 Å. Thus, a weak repulsive lone-pair−lone-pair interaction could be envisioned. We speculate that the irreversible structural change may be associated with this repulsion.

Concluding Remarks

Pb_3SeO_5 is a novel NCS and polar material, whose macroscopic polarity is wholly attributable to the SeO_3 polyhedra. Although macroscopically polar, the material is not ferroelectric, i.e., the polarization is not reversible. The material, however, does exhibit strong SHG, piezoelectric, and pyroelectric behavior. It is also of interest to note that Pb_3SeO_5 undergoes an irreversible phase transition at ~440 °C, that we speculate is attributable to weak lone-pair−lone-pair repulsions. In order to gain a deeper insight into these repulsions, we are investigating materials that contain two lone-pair cations.[80]

Acknowledgment. We thank the Welch Foundation (Grant E-1457), NSF (DMR-0652150), and ACS PRF (47345-AC10) for support.

Supporting Information Available: Additional experimental and theoretical data. This material is available free of charge via the Internet at http://pubs.acs.org.

(79) Cohen, R. E. *Nature* (*London*) **1992**, *358*, 136.

(80) Porter, Y.; Halasyamani, P. S. *Inorg. Chem.* **2003**, *42*, 205.